Interaction force and motion estimators facilitating impedance control of the upper limb rehabilitation robot

Aitziber Mancisidor[1], Asier Zubizarreta[1], Itziar Cabanes[1], Pablo Bengoa[1] and Je Hyung Jung[2]

***Abstract*— In order to enhance the performance of rehabilitation robots, it is imperative to know both force and motion caused by the interaction between user and robot. However, common direct measurement of both signals through force and motion sensors not only increases the complexity of the system but also impedes affordability of the system. As an alternative of the direct measurement, in this work, we present new force and motion estimators for the proper control of the upper-limb rehabilitation Universal Haptic Pantograph (UHP) robot. The estimators are based on the kinematic and dynamic model of the UHP and the use of signals measured by means of common low-cost sensors. In order to demonstrate the effectiveness of the estimators, several experimental tests were carried out. The force and impedance control of the UHP was implemented first by directly measuring the interaction force using accurate extra sensors and the robot performance was compared to the case where the proposed estimators replace the direct measured values. The experimental results reveal that the controller based on the estimators has similar performance to that using direct measurement (less than 1 N difference in root mean square error between two cases), indicating that the proposed force and motion estimators can facilitate implementation of interactive controller for the UHP in robot-mediated rehabilitation trainings.**

I. INTRODUCTION

Motor deficit is one of the most frequent sequels in people who have suffered a stroke, with more than 80% of survivors suffering it [1]. Nowadays, the most common way to recover these lost functionalities is to perform rehabilitation exercises for the affected limb. However, with traditional techniques, due to temporary, personal or economic limitations, in many cases, the hours of rehabilitation are limited.

In view of this situation, robotic devices have been proposed as an alternative to traditional rehabilitation procedures [2], [3], and scientific interest in this line of research has been greatly increased. As a result, many robots for both upper [4], [5] and lower limb rehabilitation [6], [7] have been proposed in the last decade.

A large part of these works focuses on the mechanical design of the devices, analyzing the type of structure (serial or exoskeleton) [8], [9], number of degrees of freedom, type of actuators [10], etc. However, a suitable and robust controller is also required to ensure that these robots interact properly with the user. An appropriate controller can lead to an enhanced performance of the robotic device, resulting in significant and fast improvement of patient status as well as shorter rehabilitation time. On the other hand the malfunction of the controller can injure the user, which is not acceptable in human-robot interaction.

Classical control strategies, such as position control, do not consider the dynamics of the interaction between the patient and the robot, so, they are not suitable for this type of applications. In order to handle this interaction, it is necessary to implement advanced control algorithms that combine motion and force measurements. Among them, the ones based on the mechanical impedance of the system, the so called impedance control [11], and its complementary, admittance control, have been mostly emerged [12].

Impedance control is based on a model-based force controller with position feedback, while its complementary, admittance control, is based on a position controller with force feedback. In both cases, they control the force/position relationship in all directions of motion. In addition, these algorithms have the ability to adapt to the recovery status of the patients, which makes them one of the best techniques for rehabilitation devices [13].

As these advanced controllers have to be able to control both interaction forces and motions, they need to measure their real values. Usually, these values are measured directly using force and position sensors. However, these approaches cause several drawbacks [14], [15]; i) mechanical and electrical difficulties in placement of sensors, ii) requiring adequate processing of sensors signals due to their noise and temperature dependency, and iii) in most cases, the price of sensors is expensive.

Another approach is the use of force and motion estimators based on the sensors available in the robot, which has been successfully implemented in several industrial robotic applications. These estimators are usually based on the measurement of the position sensors attached to the joints and the torques exerted by the actuators. Among the different estimation techniques that can be found in the bibliography, perhaps the most common one is based on the kinematic and dynamic model of the device [16], [17].

In this context, we apply the same concept to the rehabilitation robots in order to reduce the overall cost of the robot as well as the complexity of the robot. So in this work, we present interaction force and motion estimators for one

*This work was supported in part by the Basque Country Governments (GV/EJ) under grant PRE-2014-1-152, UPV/EHU's PPG17/56 project, Basque Country Governments IT914-16 project, Ministry of Economy and Competitiveness' MINECO FEDER inside DPI-2012-32882 project, Spanish Ministry of Economy and Competitiveness BES-2013-066142 grant, Euskampus, FIK and Spanish Ministry of Science and Innovation PDI-020100-2009-21 project.

[1]Aitziber Mancisidor, Asier Zubizarreta, Itziar Cabanes and Pablo Bengoa are with the Department of Automatics and System Engineering, University of the Basque Country (UPV/EHU), Plaza Ing. Torres Quevedo, Bilbao 48013, Spain asier.zubizarreta@ehu.eus

[2]Je Hyung Jung is with the Neurorehabilitation Area, Health Division, TECNALIA Research and Innovation, Mikeletegi Pasealekua, 1-3 E-20009 Donostia-San Sebastian, Spain. jehyung.jung@tecnalia.com

of upper-limb rehabilitation robots, Universal Haptic Pantograph (UHP), which has been shown in several publications [18], [19], [20]. The UHP is an innovative rehabilitation robot for complete upper limb training and used for the rehabilitation of shoulders, elbows and wrists in people who suffer motor disability after a stroke.

The rest of the article is structured as follows. In Section II, the UHP is briefly described and parameters needed for formulation of the estimators are introduced. In section III, the force and motion estimators are formulated. In Section IV, we analyze and validate the performance of these estimators in several experimental studies. For the validation, the performance of force and impedance controllers using direct measurement of interactive force is compared to that of the controllers using the estimated force and motion from the proposed estimators. Finally, the most important ideas and future work are summarized in the conclusions, Section V.

II. UNIVERSAL HAPTIC PANTOGRAPH

The Universal Haptic Pantograph (UHP) is a rehabilitation robot for training the upper limbs (Fig.1). One of its main advantages is the possibility of varying its mechanical structure through the use of three lockable/unlocking joints. This allows eight different modes of training, which can be used to rehabilitate all joints of the upper limb [18].

Fig. 1. The rehabilitation robot Universal Haptic Pantograph (UHP).

Among these eight mechanical configurations or modes of operation, this work focuses on one of the most used, the ARM mode, in which the UHP executes planar flexion/extension motions of the arm through 2 degrees of freedoms (DOF) movement in quasi x-y plane [18], allowing to rehabilitate the three movements of the shoulder (rotation, flexion/extension and abduction/adduction) and the flexion/extension movement of the elbow.

The UHP is mechanically composed of two subsystems; a drive system based on Serial Elastic Actuators (SEA) that generates force and motion (Fig. 2) and a closed pantograph-shaped structure where the user interacts the UHP (Fig. 3).

The motion of the UHP results from the forces ($\mathbf{F_{Cn}}$) exerted by the user to pantograph and the driving torques ($\boldsymbol{\tau_m}$) exerted by the motors through the drive system. The two subsystems are connected to each other, allowing them to transmit bilaterally both forces ($\mathbf{F_{Tr}}$) and motions ($\mathbf{P_{Tr}}$) shown in Figs. 2 and 3.

The drive system, which allows 2 DOFs movement of the pantograph-shaped structure in quasi x-y plane, is actuated by two perpendicular SEAs composed by two Maxon RE40 rotative motors (m_1 and m_2), four springs (S_A, S_B, S_C and S_D) and a series of pulleys with r_m radius, joined through a cable-based transmission system. As a result, the system is able to exert force ($\mathbf{F_{Tr}}$) and motion ($\mathbf{P_{Tr}}$) on the pantograph in two perpendicular directions (x and y). In each direction, the rotative motor generates a torque that is transmitted through cables to a couple of springs, which transmit the forces and motions to the point ($\mathbf{P_{Tr}}$) of the pantograph as shown in Fig. 2.

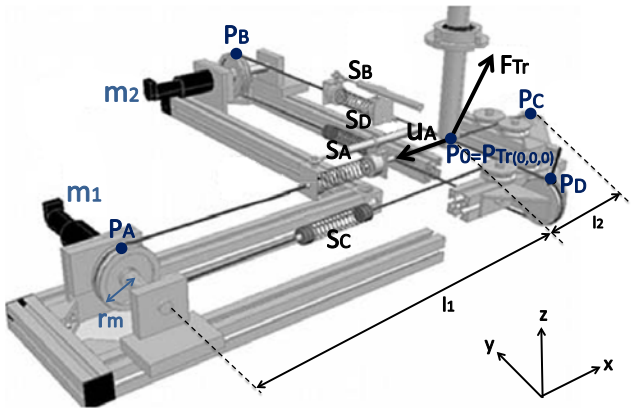

Fig. 2. The drive system of the UHP. In the figure, y axis denotes forward-backward motion of the pantograph and x axis leftward-rightward motion. ($\mathbf{P_0}$ and $\mathbf{P_{Tr}}$ in this figure correspond to those in Fig. 3).

The pantograph is composed of a fixed structure and three mobile bars (actuated, transverse and parallel) as shown in Fig. 3. These bars are connected by five joints ($\mathbf{P_E}$, $\mathbf{P_F}$, $\mathbf{F_G}$, $\mathbf{P_H}$ and $\mathbf{P_I}$), where $\mathbf{P_F}$, $\mathbf{P_H}$ and $\mathbf{P_I}$ are lockable/unlockable. Also, note that the pantograph is actuated by the drive system in the transmission point ($\mathbf{P_{Tr}}$) and by the user in the contact point ($\mathbf{P_{Cn}}$).

In ARM mode, joint $\mathbf{P_F}$ is locked, so the actuated bar actuates as a single stiff link from $\mathbf{P_{Tr}}$ to $\mathbf{P_G}$. Furthermore, joints $\mathbf{P_H}$ and $\mathbf{P_I}$ are unlocked, in order to allow the motion of the transverse and parallel bars. This way, a four bar mechanism structure is defined, where, parallel and actuated bars are always transverse.

On the other hand, the equilibrium position of the UHP is achieved when the actuated bar is in vertical position,

defining the origin ($\mathbf{P_0}$) of the base reference frame appearing Figs. 2 and 3.

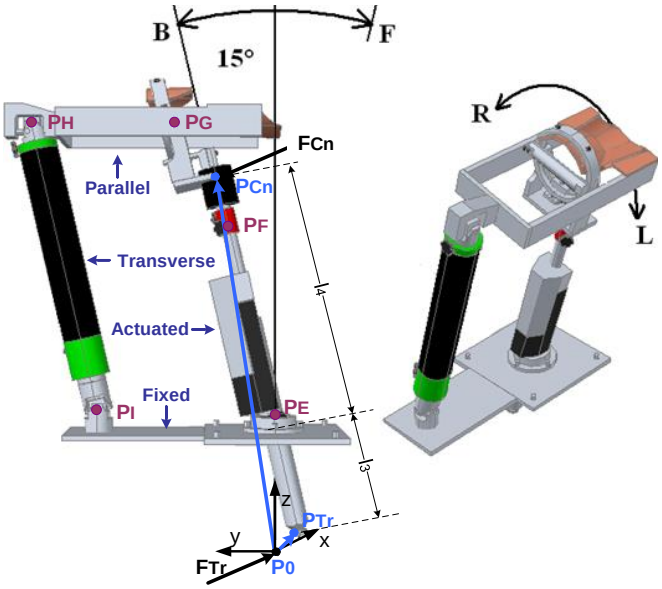

Fig. 3. Pantograph structure in ARM mode (Joint $\mathbf{P_F}$ is locked while joints $\mathbf{P_H}$ and $\mathbf{P_I}$ are free). It perform quasi-planar movements in Forward/Backward/Leftward/Rightward directions.

III. FORCE AND MOTION ESTIMATORS FOR PROPER IMPEDANCE CONTROL

An impedance controller for UHP has been designed to perform tasks usually employed in the rehabilitation trainings and it appears in Fig. 4. As mentioned in the introduction of this article, the impedance controller controls the dynamic relationship between the force ($\mathbf{F_{Cn}}$) and the motion ($\mathbf{P_{Cn}}$) of the contact point. It calculates the desired contact force ($\mathbf{F_{Cn_{Des}}}$) in terms of the error between the desired ($\mathbf{P_{Cn_{Des}}}$) and actual ($\mathbf{P_{Cn}}$) contact point position.

$$\mathbf{F_{Cn_{Des}}}(s) = (\mathbf{K_d} + \mathbf{B_d}\ s + \mathbf{M_d}\ s^2)(\mathbf{P_{Cn_{Des}}}(s) - \mathbf{P_{Cn}}(s)) \quad (1)$$

where $\mathbf{K_d}$ is the stiffness matrix, $\mathbf{B_d}$ is the damping matrix and $\mathbf{M_d}$ is the inertial matrix, which define the desired impedance of the robot.

Once the desired contact force ($\mathbf{F_{Cn_{Des}}}$) is decided by (1), the force controller is adopted to ensure that actual contact force ($\mathbf{F_{Cn}}$) tracks the desired one ($\mathbf{F_{Cn_{Des}}}$) and output of the controller is an actuator torque ($\boldsymbol{\tau_m}$) of the drive system. Commonly, the actual contact force ($\mathbf{F_{Cn}}$) required for the force controller has been directly measured by highly qualified force sensor. This approach, however, increases not only the cost of the device but also complexity of mechanical an electrical setup. To resolve those drawbacks, therefore, we formulate and use the force estimator, which can be used to replace the sensors.

The proposed force estimator uses the dynamic model of the UHP and signals basically measured by common low-cost sensors already implemented in the UHP: the two optical encoders integrated in the rotary motors (q_{m_1} and q_{m_2}), and two linear potentiometers that measure the variable length (n_{S_A} and n_{S_B}) of the springs S_A and S_B. In addition, those signals are used to estimate contact point ($\mathbf{P_{Cn}}$), resulting in a motion estimator. The proposed estimators will be detailed in the following subsection.

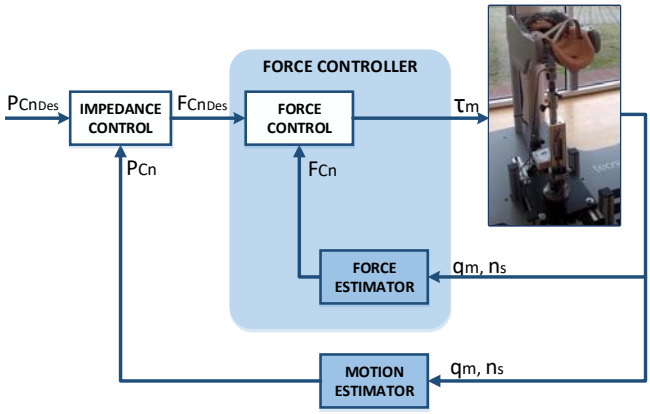

Fig. 4. Impedance control of the UHP rehabilitation robot with force and motion estimators.

A. Motion Estimator

The proposed estimator aims to calculate the actual position of the contact point ($\mathbf{P_{Cn}}$) based on the kinematic model of the UHP and the measured signals (n_{S_A}, n_{S_B}, q_{m_1} and q_{m_2}) from the common encoders and linear potentiometers.

In ARM mode of UHP from Fig. 3, by its specific geometry, the contact point ($\mathbf{P_{Cn}}$) relates to transmission point ($\mathbf{P_{Tr}}$) as

$$\mathbf{P_{Cn}} = -\frac{l_3}{l_4}\mathbf{P_{Tr}} \quad (2)$$

where l_3 is the distance between the transmission point ($\mathbf{P_{Tr}}$) and joint $\mathbf{P_F}$ and l_4 is the distance between joint $\mathbf{P_F}$ and contact point ($\mathbf{P_{Cn}}$).

Hence, as first step, the transmission point ($\mathbf{P_{Tr}} = [x_{Tr}\ y_{Tr}\ z_{Tr}]^T$ is formulated from the drive system (Fig. 2) and then contact point ($\mathbf{P_{Cn}}$) is computed by (2).

From the analysis of the drive system shown in Fig. 2, the variable length of springs S_A and S_B, n_{S_A} and n_{S_B}, are obtained as

$$\begin{aligned} n_{S_A} &= l_A + q_{m_1} r_m - l_1 \\ n_{S_B} &= l_B + q_{m_2} r_m - l_1 \end{aligned} \quad (3)$$

where l_1 is distance between the motors and equilibrium position of the transmission point ($\mathbf{P_0}$), r_m is the radius of the pulleys, l_A is the distance between the point $\mathbf{P_A}$ and $\mathbf{P_{Tr}}$, and l_B the distance between the point $\mathbf{P_B}$ and $\mathbf{P_{Tr}}$. The values of l_A and l_B can be calculated depending on the motion of the transmission point,

$$\begin{aligned} l_A &= \mathbf{P_A P_{Tr}} = \sqrt{(l_1 + x_{Tr})^2 + y_{Tr}^2} \\ l_B &= \mathbf{P_B P_{Tr}} = \sqrt{x_{Tr}^2 + (l_1 - y_{Tr})^2} \end{aligned} \quad (4)$$

Combining (3) and (4),

$$\begin{aligned}\sqrt{(l_1+x_{Tr})^2+y_{Tr}^2} &= n_{S_A}-q_{m_1}r_m+l_1\\ \sqrt{x_{Tr}^2+(l_1-y_{Tr})^2} &= n_{S_B}-q_{m_2}r_m+l_1\end{aligned} \tag{5}$$

In addition, from Fig. 3, $\mathbf{P_{Tr}}$ motion is constrained by spherical joint ($\mathbf{P_E}$), resulting in constrained spherical motion as

$$x_{Tr}^2+y_{Tr}^2+(l_3-z_{Tr})^2=l_3^2 \tag{6}$$

Solving three equations in (5) and (6), spatial coordinate ($[x_{Tr}\ y_{Tr}\ z_{Tr}]^T$) of $\mathbf{P_{Tr}}$ is computed and finally $\mathbf{P_{Cn}}$ is obtained by (2). As shown in above equations, $\mathbf{P_{Cn}}$ is computed by using only rotation angle (q_{m_1} and q_{m_2}) of the motors and the variable length (n_{S_A} and n_{S_B}) of the upper springs.

B. Contact Force Estimator

Once the motion of the contact point ($\mathbf{P_{Cn}}$) is known, the contact force ($\mathbf{F_{Cn}}$) on that point ($\mathbf{P_{Cn}}$) can be estimated based on the dynamic model of the UHP, the position of $\mathbf{P_{Cn}}$ and the measured signals (n_{S_A}, n_{S_B}, q_{m_1} and q_{m_2}) by means of the same sensors used for the motion estimator.

Similarly in the motion estimator, the contact force ($\mathbf{F_{Cn}}$) and the transmission force ($\mathbf{F_{Tr}}$) has a specific relation due to particular geometry of UHP in ARM mode, from Fig. 3,

$$\mathbf{F_{Cn}}=\mathbf{T_{ARM}}\,\mathbf{F_{Tr}} \tag{7}$$

where $\mathbf{T_{ARM}}$ is the transformation matrix expressing by

$$\mathbf{T_{ARM}}=-\frac{l_3}{l_4}\mathbf{I}_{3x3} \tag{8}$$

where l_3 is the distance between the transmission point ($\mathbf{P_{Tr}}$) and joint $\mathbf{P_F}$, l_4 is the distance between joint $\mathbf{P_F}$ and contact point ($\mathbf{P_{Cn}}$), and $\mathbf{I}_{3x3}$ is the identity matrix of dimension 3.

On the other hand, from the dynamic analysis of the drive system it is obtained that the transmission force ($\mathbf{F_{Tr}}$) is the sum of the forces exerted by the four springs connected to the transmission point ($\mathbf{P_{Tr}}$) as shown in Fig. 2,

$$\mathbf{F_{Tr}}=\mathbf{F}_{S_A}+\mathbf{F}_{S_B}+\mathbf{F}_{S_C}+\mathbf{F}_{S_D}=\sum_{i=A}^{D}\mathbf{F}_{S_i} \tag{9}$$

The magnitude of each spring force (F_{Si}) depends on its constant (k_{S_i}) and its variable length (n_{S_i}), while its direction ($\mathbf{u}_i$) depends on the transmission motion ($\mathbf{P_{Tr}}$).

$$\mathbf{F}_{Si}=F_{S_i}\,\mathbf{u}_i=k_{S_i}\,n_{S_i}\,\mathbf{u}_i \tag{10}$$

where $\mathbf{u}_i$ is the unitary direction vector of $\mathbf{P_{Tr}P_i}$ for i = A, B, C, D (Fig. 2).

In (10), two parameters, n_{S_C} and n_{S_D}, are still unknown and they can be computed in the same way applied to obtain n_{S_A} and n_{S_B}. By analyzing geometry of the drive system in the Fig. 2,

$$\begin{aligned}n_{S_C} &= l_C+q_{m_1}r_m-l_2\\ n_{S_D} &= l_D+q_{m_2}r_m-l_2\end{aligned} \tag{11}$$

where r_m is the radius of the pulleys, l_2 is the distance between the equilibrium position ($\mathbf{P_0}$) of the transmission point and the point $\mathbf{P_C}$ (or $\mathbf{P_D}$) on the un-actuated pulleys, l_C is the distance between point $\mathbf{P_C}$ and $\mathbf{P_{Tr}}$, and l_D is the distance between points $\mathbf{P_D}$ and $\mathbf{P_{Tr}}$. In addition, l_C and l_D can be calculated as

$$\begin{aligned}l_C &= \mathbf{P_CP_{Tr}} &= \sqrt{(x_{Tr}-l_2)^2+y_{Tr}^2}\\ l_D &= \mathbf{P_DP_{Tr}} &= \sqrt{x_{Tr}^2+(l_2+y_{Tr})^2}\end{aligned} \tag{12}$$

Hence, combining (7) - (12), contact position ($\mathbf{P_{Cn}}$) and measured signals from the encoders and linear potentiometers yields the estimation of the contact force ($\mathbf{F_{Cn}}$).

IV. VALIDATION RESULTS

Three experimental tests were carried out to demonstrate the effectiveness of the proposed force and motion estimators. In the first two tests, in order to validate the force estimator, only the force controller was used, while in the last one the impedance controller was used. In the tests, we compare the performance of the controller with the proposed estimators to that of controller with additional MINI40 force sensor (ATI, $6DOF$, $1/100N$ resolution) and YNGS1 inclinometer (Sensor-Technik Wiedemann GmbH, $3DOF$, $0.25/s$ resolution) that directly measure the contact position and force.

In order to use the estimators, the geometric parameters of the UHP were experimentally identified and summarized in Table I.

TABLE I
PARAMETERS OF THE UHP PROTOTYPE.

Parameter	Value
r_m	$0.047m$
k_{S_i}	$4000N/m$
l_1	$0.575m$
l_2	$0.15m$
l_3	$0.18m$
l_4	$0.46m$

The first test aims to verify that the force controller using the force estimator works properly, meaning good force tracking performance with respect to variable contact forces. Hence the motion of the contact point ($\mathbf{P_{Cn}}$) was locked while variable desired contact force ($\mathbf{F_{Cn_{Des}}}$) was applied, which emulates an exercise that patient tries to maintain the robot position constant from perturbations.

Usually, the UHP works with frequencies between 0.1 and $1Hz$ [20]. So, for this test, as contact force reference, three sinusoidal signals of amplitude $10N$ with period of 10, 5 and 1 seconds were selected. Fig. 5 shows the desired contact force ($\mathbf{F_{Cn_{Des}}}$) in the x direction and the actual contact force obtained by the force controller with force sensor ($\mathbf{F_{Cn_{Sensor}}}$) and with the estimator ($\mathbf{F_{Cn_{Estimator}}}$).

As it can be seen, in all cases, the controller was able to follow the desired force reference changes with small

errors. In the case of the controller with sensor the root mean square (RMS) error of the three signs is $2.17N$ while with the estimator it is $2.22N$.

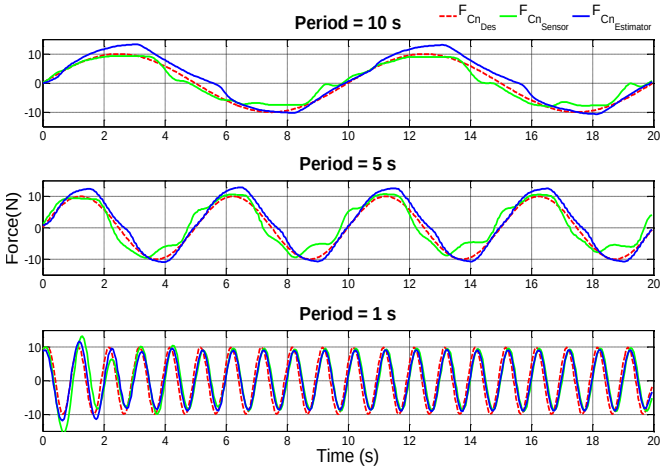

Fig. 5. **Test 1**: Validation of the force controller based on force estimation with force references having different period of 10, 5 and 1 seconds.

In the second test, the desired contact force was set to zero ($\mathbf{F_{Cn_{Des}}} = \mathbf{0}N$) while the user randomly moved UHP in x and y directions with approximate speed of $1m/s$ in the range of motion, which presents so-called zero impedance or transparent mode that enables the patient to move the device with very low device inertia and friction.

Fig. 6 shows the desired contact force ($\mathbf{F_{Cn_{Des}}}$), and the response of the force controller with force sensor ($\mathbf{F_{Cn_{Sensor}}}$) and based on estimator ($\mathbf{F_{Cn_{Estimator}}}$) in the y axis.

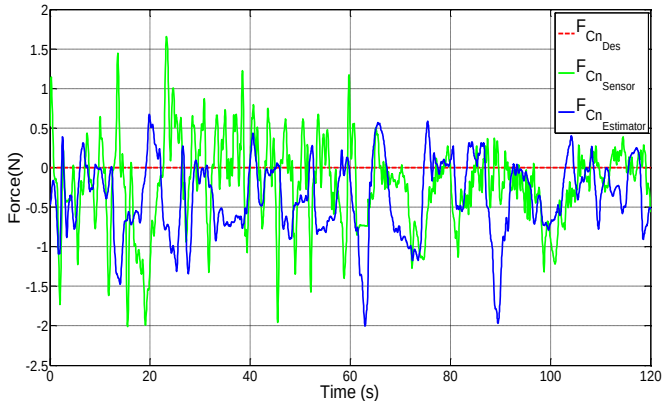

Fig. 6. **Test 2**: Validation of the force controller based on force estimation with zero force reference.

As it can be seen, the performance with both control responses is similar. In case of the use of the force sensor, RMS error is $0.58N$ and the maximum is $2.01N$, while with the estimator, RMS and the maximum error are $0.61N$ and $2N$, respectively.

Finally the impedance controller was used to validate the entire control system with force and motion estimators, which has been widely adopted in rehabilitation robots. In the impedance controller (1), the desired contact force ($\mathbf{F_{Cn_{Des}}}$) was calculated in terms of the error between the desired ($\mathbf{P_{Cn_{Des}}}$) and actual ($\mathbf{P_{Cn}}$) position of the contact point.

In Fig. 7, the results of the impedance controller in the direction of the trajectory using force and motion sensors are shown, while the results of the impedance controller based on force and motion estimators are illustrated in Fig. 8. The desired motion profiles shown in Figs. 7 and 8 were composed of random combination of different step inputs with $0.14m$, $0.11m$ and $0.05m$ magnitudes in order to reflect more realistic rehabilitation exercises performed by UHP.

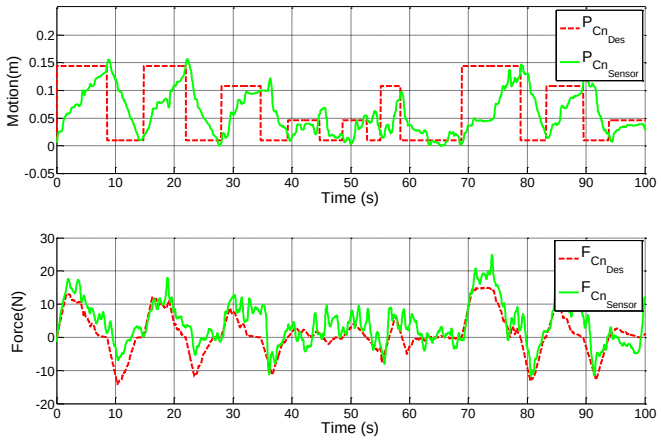

Fig. 7. **Test 3**: Results of the impedance controller with force and motion sensors.

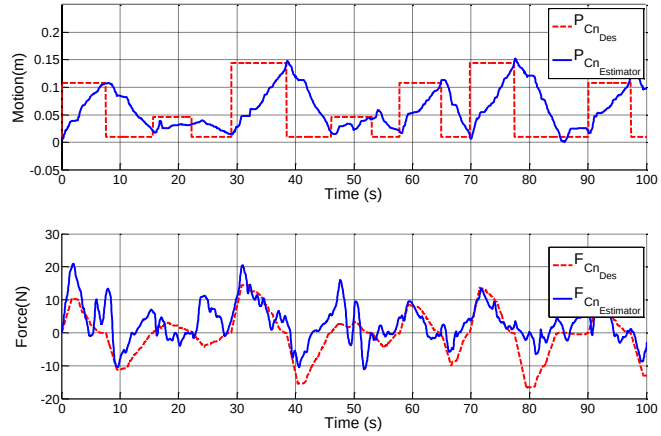

Fig. 8. **Test 3**: Results of the impedance controller with force and motion estimators.

In both cases, the UHP assisted the user to reach the desired point ($\mathbf{P_{Cn_{Des}}}$) performing gentle and robust motions with the compliance calculated by the impedance controller (1). In addition, with both methods, the controller was able to follow the desired force reference with small errors. In the case of the controller with the sensors RMS error is $4.92N$, while with the estimators it is $5.84N$.

As it can be seen in Table II, the controller based on the sensor shows a little better performance than that with force and motion estimators. However, the difference of tracking errors between two cases is $0.05N$ in first test, $0.03N$

in second test, and $0.92N$ in last test, indicating that the performance of the estimators is acceptable.

TABLE II
ROOT MEAN SQUARE ERROR OF FORCE.

	With the sensor			**With the estimator**		
Test 1	**10s**	**5s**	**1s**	**10s**	**5s**	**1s**
	$1.94N$	$1.71N$	$2.85N$	$1.61N$	$2.41N$	$2.61N$
Test 2	$0.58N$			$0.61N$		
Test 3	$4.92N$			$5.84N$		

It would be worth noting that in assistive and sanitary applications, the compliance and safety of the device are more critical aspect than accurate trajectory tracking, which is may be of importance in other applications of robotics. For instance, depending on the impairment level of the patient as well as the type of demanded exercises for rehabilitation, RMS errors of position and force below $1cm$ and $6N$, which were obtained in the experimental tests, might be acceptable.

From the experimental results, the proposed force and motion estimators can be used in human-robot interactive controller such as impedance controller in place of expensive high-qualified sensors like 6 axis force-torque sensor, allowing an affordable robotic solution for rehabilitation.

V. CONCLUSIONS

In this work new force and motion estimators for proper impedance control of the rehabilitation robot Universal Haptic Pantograph (UHP) were presented. The main objective of these estimators is to replace extra force and position sensors that add mechanical and electronical complexity of the device as well as decrease the affordability of the device. The proposed estimators are based on the kinematic and dynamic model of the UHP and the signals measured by common angle and position sensors already implemented in the UHP, which are two optical encoders and two linear potentiometers for measurement of the rotation angle of the motors and variable length of two springs respectively.

To verify the performance of the controller using the proposed force and motion estimators, three experimental tests were carried out. The results show that the use of the estimators produces less than $1N$ difference in terms of mean force tracking error compared to the case where the controller uses directly measured signals by the sensors. In addition, gentle and robust motions of the UHP with the estimator were observed in the tests while UHP well tracked desired force profiles within the mean error of $6N$.

The results indicate that the estimators would be suitable for the interactive controller design of the UHP in real applications and the clinical trials of the UHP adopting the estimators with patients will be of future interest.

REFERENCES

[1] B. Sheng, Y. Zhang, W. Meng, C. Deng, and S. Xie, "Bilateral robots for upper-limb stroke rehabilitation: State of the art and future prospects," *Medical Engineering & Physics*, vol. 38, no. 7, pp. 587–606, 2016.

[2] S. Xie, "Advanced Robotics for Medical Rehabilitation," *Springer Tracts in Advanced Robotics*, vol. 108, pp. 1–357, 2016.

[3] S.-H. Zhou, J. Fong, V. Crocher, Y. Tan, D. Oetomo, and I. Mareels, "Learning control in robot-assisted rehabilitation of motor skills a review," *Journal of Control and Decision*, vol. 3, no. 1, pp. 19–43, 2016.

[4] J. Brackenridge, L. V. Bradnam, S. Lennon, J. J. Costi, and D. A. Hobbs, "A Review of Rehabilitation Devices to Promote Upper Limb Function Following Stroke," *Neuroscience and Biomedical Engineering*, vol. 4, no. 1, pp. 25–42, 2016.

[5] T. Proietti, V. Crocher, A. Roby-Brami, and N. Jarrasse, "Upper-limb robotic exoskeletons for neurorehabilitation: a review on control strategies," *IEEE Reviews in Biomedical Engineering*, vol. 9, pp. 4–14, 2016.

[6] W. Meng, Q. Liu, Z. Zhou, Q. Ai, B. Sheng, and S. S. Xie, "Recent development of mechanisms and control strategies for robot-assisted lower limb rehabilitation," *Mechatronics*, vol. 31, pp. 132–145, 2015.

[7] T. Yan, M. Cempini, C. M. Oddo, and N. Vitiello, "Review of assistive strategies in powered lower limb orthoses and exoskeletons," *Robotics and Autonomous Systems*, vol. 64, pp. 120–136, 2015.

[8] R. A. R. C. Gopura, D. S. V. Bandara, K. Kiguchi, and G. K. I. Mann, "Developments in hardware systems of active upper-limb exoskeleton robots: A review," *Robotics and Autonomous Systems*, vol. 75, pp. 203–220, 2016.

[9] M. Babaiasl, S. H. Mahdioun, P. Jaryani, and M. Yazdani, "A review of technological and clinical aspects of robot-aided rehabilitation of upper-extremity after stroke," *Disability and Rehabilitation: Assistive Technology*, pp. 1–18, jan 2015.

[10] A. J. Veale and S. Q. Xie, "Towards compliant and wearable robotic orthoses: A review of current and emerging actuator technologies," *Medical Engineering & Physics*, vol. 38, no. 4, pp. 317–325, 2016.

[11] N. Hogan, "Impedance Control: An Approach to Manipulation," *Journal of Dynamic Systems, Measurement, and Control*, vol. 107, no. 1, 1985.

[12] N. Nordin, S.-q. Xie, and B. Wünsche, "Assessment of movement quality in robot- assisted upper limb rehabilitation after stroke: a review," *Journal of NeuroEngineering and Rehabilitation*, vol. 11:137, no. 1, pp. 1–23, 2014.

[13] N. Jarrassé, T. Proietti, V. Crocher, J. Robertson, A. Sahbani, G. Morel, and A. Roby-Brami, "Robotic Exoskeletons: A Perspective for the Rehabilitation of Arm Coordination in Stroke Patients," *Frontiers in Human Neuroscience*, vol. 8, no. 947, pp. 1–13, 2014.

[14] S. Etedali, H. A. Talebi, and A. D. Mohammadi, "A robust force observer for robot manipulators subjected to external disturbance," *International Conference on Robotics and Mechatronics (ICROM)*, no. 1, pp. 539–544, 2015.

[15] H. Amini, V. Dabbagh, S. M. Rezaei, M. Zareinejad, N. A. Mardi, and A. A. D. Sarhan, "Robust control-based linear bilateral teleoperation system without force sensor," *Journal of the Brazilian Society of Mechanical Sciences and Engineering*, vol. 37, no. 2, pp. 579–587, 2015.

[16] A. Colome, D. Pardo, G. Alenya, and C. Torras, "External force estimation during compliant robot manipulation," *International Conference on Robotics and Automation*, pp. 3535–3540, 2013.

[17] M. Linderoth, A. Stolt, A. Robertsson, and R. Johansson, "Robotic force estimation using motor torques and modeling of low velocity friction disturbances," *International Conference on Intelligent Robots and Systems*, pp. 3550–3556, 2013.

[18] J. C. Perry, J. Oblak, J. H. Jung, I. Cikajlo, J. F. Veneman, N. Goljar, N. Bizoviar, Z. Matjai, and T. Keller, "Variable structure pantograph mechanism with spring suspension system for comprehensive upper-limb haptic movement training," *The Journal of Rehabilitation Research and Development*, vol. 48, no. 4, pp. 317–334, 2011.

[19] J. Oblak and Z. Matjačić, "Design of a series visco-elastic actuator for multi-purpose rehabilitation haptic device.," *Journal of neuroengineering and rehabilitation*, vol. 8:3, pp. 1–13, 2011.

[20] J. Oblak, I. Cikajlo, T. Keller, J. C. Perrry, J. Veneman, and Z. Matja, "The Role of Viscous Damping on Quality of Haptic Interaction in Upper Limb Rehabilitation Robot : A Simulation Study," *IFMBE Proceedings*, pp. 383–386, 2010.